Available online at www.sciencedirect.com
ScienceDirect
Journal of the European Ceramic Society 31 (2011) 2931–2938
www.elsevier.com/locate/jeurceramsoc

Sintering and oxygen permeation studies of $La_{0.6}Sr_{0.4}Co_{0.2}Fe_{0.8}O_{3-\delta}$ ceramic membranes with improved purity

Yuan Zou [a], Wei Zhou [b], Shaomin Liu [c], Zongping Shao [a,*]

[a] *State Key Laboratory of Materials-Oriented Chemical Engineering, College of Chemistry & Chemical Engineering, Nanjing University of Technology, No. 5 Xin Mofan Road, Nanjing 210009, PR China*
[b] *School of Chemical Engineering, The University of Queensland, Brisbane, Queensland 4072, Australia*
[c] *Department of Chemical Engineering, Curtin University of Technology, Perth, WA 6845, Australia*

Received 6 April 2011; received in revised form 21 July 2011; accepted 24 July 2011
Available online 15 August 2011

Abstract

High purity raw materials are used for synthesizing $La_{0.6}Sr_{0.4}Co_{0.2}Fe_{0.8}O_{3-\delta}$ (LSCF6428) powders to reduce the effect of impurity phases on oxygen permeability of the corresponding membranes. The as-synthesized LSCF6428 powders require a sintering temperature above 1180 °C to achieve membrane density over 90%. Ball milling of the powders increases the membrane sintering. It also increases oxygen permeation flux from 0.37 to 0.43 ml cm^{-2} min^{-1} at 950 °C for the membranes sintered at 1100 °C. A decrease in oxygen permeation fluxes with the further increase in sintering temperature is observed for the membranes with ball-milled starting powders, accompanied by an obvious increase in grain size. It suggests, at low level of impurity phases, the grain boundaries facilitate the oxygen diffusion. The combination of ball milling of the starting powders and a sintering temperature of 1100 °C is optimal to achieve high oxygen permeability of LSCF6428 membranes with improved purity.

Keywords: Impurities; Sintering; Grain boundaries; Membranes; Oxygen permeation

1. Introduction

Oxygen is an important industrial gas with applications in various important fields.[1–4] It is generally believed that the market demand on oxygen will be substantially expanded in the near future.[5] Chemical potential driven oxygen separation using dense ceramic or cermet membranes represents one promising technology for future oxygen production industry.[6–11] The oxygen-permeating membranes, which are in dense type and made of mixed oxygen ionic and electronic conducting single phase oxides, composite oxides or cermets, allow only oxygen ion and electron to diffuse through. Thus, theoretically, continuous oxygen separation with 100% oxygen selectivity can be easily reached if there is a certain oxygen gradient across the membrane.

The oxygen permeability of ceramic membranes is directly related to their materials composition. It is well known that the oxygen permeation flux is a function of oxygen-ionic conductivity and also the electronic conductivity, which are determined by the materials composition and the lattice structure. Recently it was found that the oxygen permeability is also closely related to the membrane microstructure. Most of the current ceramic oxygen-permeating membranes are constructed from polycrystalline oxides, and the grain boundary diffusion plays an important role in the oxygen permeation process. A change in grain size may significantly affect the oxygen permeation behavior of the membranes. For many years, there have been continuous studies on this grain size effect on oxygen permeability in the fields of mixed ionic-electronic conductivity ceramics,[12,13] leading to some different conclusions. For example, some materials like $La_{0.5}Sr_{0.5}Fe_{0.1}O_{3-\delta}$,[14] $La_{0.1}Sr_{0.9}Co_{0.9}Fe_{0.1}O_{3-\delta}$[15] and $SrCo_{0.8}Fe_{0.2}O_{3-\delta}$[16] were demonstrated to have faster oxygen diffusion paths around the grain boundaries than the grain bulks, while some other perovskite oxides such as $CaTi_{0.8}Fe_{0.2}O_{3-\delta}$,[17]

* Corresponding author. Tel.: +86 25 83172256; fax: +86 25 83172242.
E-mail address: shaozp@njut.edu.cn (Z. Shao).

0955-2219/$ – see front matter © 2011 Elsevier Ltd. All rights reserved.
doi:10.1016/j.jeurceramsoc.2011.07.028

Table 1
The abbreviations of samples and the sintering status of membranes.

Sample classification	No treatment			Ball milling treatment		
Powders	OP			MP		
Membranes	M-OP-1100	M-OP-1180	M-OP-1300	M-MP-1100	M-MP-1180	M-MP-1300
Relative density (%)	86.1	91.7	95.4	90.6	93.2	95.5
Relative shrinkage (%)	16.13	18.53	18.7	16.33	18.60	19.2

$Ba_{0.5}Sr_{0.5}Co_{0.8}Fe_{0.2}O_{3-\delta}$[18] and $Ba_{0.5}Sr_{0.5}Fe_{0.8}Zn_{0.2}O_{3-\delta}$[19] were demonstrated to have the opposite effect. It suggests the complicated process for the oxygen permeation through ceramic membranes composed of polycrystalline grains.[12] Interestingly, some controversy conclusions on the grain size effect on the oxygen permeability of the membranes were reported in literature. For example, Baumanna et al. observed that $Ba_{0.5}Sr_{0.5}Co_{0.8}Fe_{0.2}O_{3-\delta}$ (BSCF) showed slight decrease in oxygen permeation flux with the increase of grain size from 10 μm up to 30 μm, and then the flux was stabilized with the further increase in grain size to 45 μm. Their results suggest the membrane microstructure actually do not have significant effect on the oxygen permeability.[20] However, Wang et al. reported a significant increase in oxygen permeation flux with the increasing grain size for the BSCF membrane.[21] Thus, a further investigation for the grain size effect on the membrane permeability is needed.

Perovskite-type $La_{0.6}Sr_{0.4}Co_{0.2}Fe_{0.8}O_{3-\delta}$ (LSCF6428) is one of the most investigated oxide materials for ceramic oxygen-permeating membranes,[22–27] which shows favorable oxygen permeability and high chemical stability at elevated temperature. Previously, by applying complexing sol–gel synthesis of the powder precursors, we found that the oxygen permeation flux of the corresponding membranes increased with the increase of grain size, created by increasing the sintering temperature.[28] It implies that the grain boundary diffusion is slower than the bulk diffusion for the LSCF6428 membrane. It is further proposed that impurity phases accumulated at the grain boundaries, which likely cause a block for the electron and oxygen ion diffusion.

In this study, LSCF6428 powders were synthesized using high-purity raw materials to minimize the impurity phases, and the sintering behavior of the related membranes was investigated. High-energy ball milling process was applied to some powders for assisting the membrane sintering to obtain membranes with different grain sizes at lower temperature. The effect of grain size on the oxygen permeability of the membranes were systematically investigated and explained.

2. Experimental

2.1. Synthesis and fabrication

The fabrication procedure for the LSCF6428 membranes with or without the introduction of a ball milling process is schematically shown in Fig. 1. Phase pure LSCF6428 powders were first prepared by an EDTA-citrate complexing sol–gel method with the detail information reported in our previous publication.[28] During the synthesis, high purity $La(NO_3)_3$, $Sr(NO_3)_2$, $Co(NO_3)_2$, and $Fe(NO_3)_3$ (metal purity > 99.99%) were applied as the cation sources, and the molar ratio of total metal ions to EDTA to citric acid was set at 1:1:2. A final calcination of the solid precursor from the sol–gel process at 800 °C for 5 h in air was conducted to obtain the LSCF6428 powders for the following processing.

Ball milling treatment of the as-synthesized powders was conducted for the purpose of improving the powder sinterability. The as-synthesized LSCF6428 powders (800 °C calcined), named as OP, was directly subjected for ball milling and the resulted powders were named as MP. To perform the powder milling, a high energy planetary ball mill (Fritsch, Pulverisette 6, Germany) with zirconia pot of 80 ml in size was used. Milling duration and rotational speed were fixed at 2 h and 400 rpm, respectively. Zirconia balls were used as milling medium. The ball to powder ratio (BPR) calculated in weight was fixed at 15:1. Ethanol was used as the liquid medium as well as the surfactant which absorbed on the particles to prevent excessive cold welding. The milling was operated at room temperature, however, in order to avoid pronounced temperature rise, 30 min of milling was alternated with 10 min of cooling.

To prepare the membranes, the original or ball-milled LSCF6428 powders were then formed into the green disk-shape membranes with a diameter of 15 mm using a stainless steel die under a hydraulic pressure of ~150 MPa. Those green membranes were subsequently sintered at 1100, 1180 or 1300 °C for 5 h. The as-obtained membranes from the powders of OP, MP are named as M-OP-*T* and M-MP-*T*, respectively, where *T* means the value of the sintering temperature for the membranes.

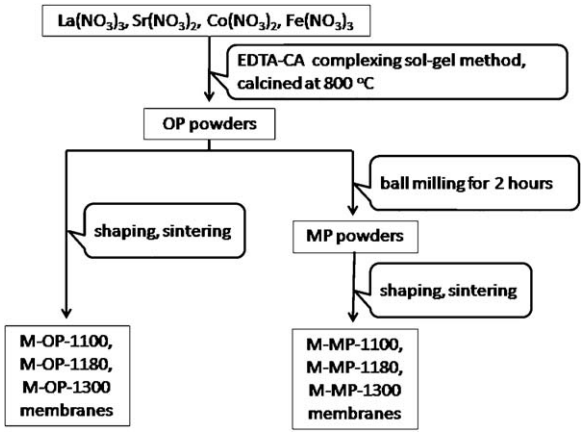

Fig. 1. The flow chart of LSCF6428 powder synthesis and subsequent membrane sintering procedure with or without conducting the ball milling treatment.

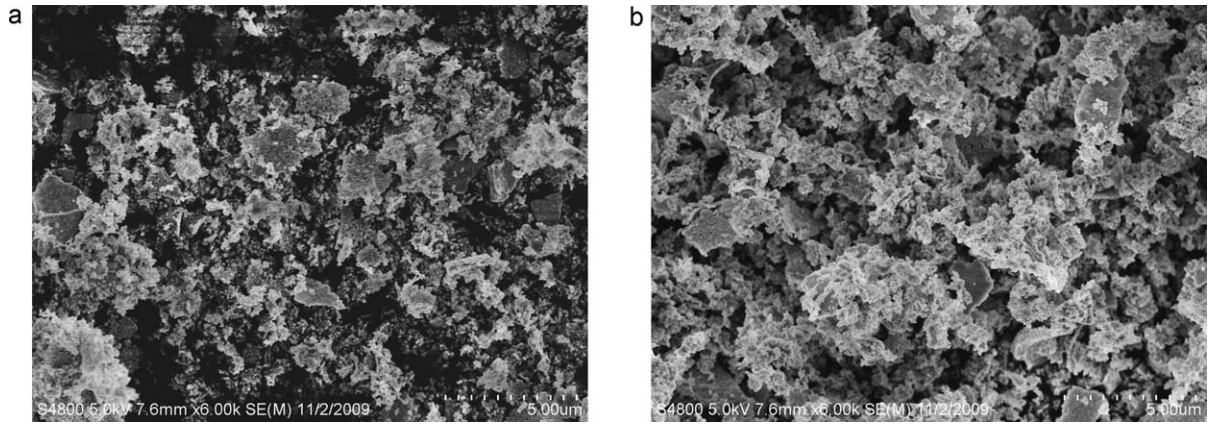

Fig. 2. The morphologies of LSCF6428 powders: (a) the original powders, and (b) the ball-milled powders.

The detail information about the abbreviations and membranes fabrication conditions is listed in Table 1.

2.2. Basic characterization

Phase structure of the membranes was investigated by using a Bruker D8 Advance diffractometer equipped with CuKα radiation (λ = 1.5418 Å). The experimental diffraction patterns were collected at room temperature by step scanning in the range of $10^\circ \leq 2\theta \leq 90^\circ$. Particle size distributions of the original and ball-milled powders were determined using a laser particle size analyzer (LPSA, Microtrac S3500, USA). Powders were dispersed in water with ultrasonic treatment for 30 min before the measurement. A field emission scanning electron microscopy (FESEM, Model Hitachi S4800) was used to observe the powder morphologies and an environmental scanning electron microscopy (ESEM, Model QUANTA-2000, FEI Company, Hillsboro, OR) was used to investigate the bulk grain morphologies of the membranes. Bulk grain size distributions were auto calculated by software utilizing these SEM graphs. An energy-dispersive X-ray spectroscopy (EDS, EDAX Company, Ametek) was used to identify the elemental composition of the milling balls and the sintered membranes from ball-milled powders to examine the purity of the as prepared membranes.

The relative density of the sintered membranes was determined by the Archimedes' water displacement method. Before measurement, membranes were boiled in water for 30 min, making the inner open pores of membranes filled with water and the saturated membranes were thus obtained. The relative density D was calculated through the following equation:

$$\rho_c = \frac{w_1}{w_3 - w_2}\rho_{H_2O} \quad (1)$$

$$D = \frac{\rho_c}{\rho_t} \times 100\% \quad (2)$$

where w_1 is the weight of the dry membrane measured in air before boiling in water. w_2 is the weight of the saturated membrane measured when it is immersed in water. And w_3 is the weight of the above saturated membrane measured in air, too. ρ_{H_2O}, ρ_c, ρ_t is the theoretical density of water at room temperature, the as calculated density of the sintered membrane, and the theoretical density of LSCF6428 membranes calculated according to the XRD spectra, respectively.

2.3. Oxygen permeation tests

The sintered disc-shape membranes were carefully polished with sand paper of 1000 mesh to a thickness of 0.9 mm. Oxygen permeation fluxes of these membranes were measured by using a setup described elsewhere.[29] A split tubular furnace was used to create operation temperature ranging from 950 to 850 °C at an interval of 25 °C per step. Two measurements were repeated to obtain the average oxygen permeation data. Ambient air was used in the feed side and high purity helium as the sweeping gas to carry the permeated oxygen to a gas chromatograph (Varian, CP3800, USA) equipped with a 5 Å molecular sieve capillary column for in situ gas composition analysis. The oxygen permeation flux was calculated by the following equation:

$$J_{O_2}(\text{mol cm}^{-2}\,\text{s}^{-1}, \text{STP}) = \left[C_O - \frac{C_N \times 0.21}{0.79} \times \left(\frac{28}{32}\right)^{1/2}\right] \times \frac{F}{S}$$

where C_O and C_N are the measured concentrations of oxygen and nitrogen in the gas on the sweep side (mol ml^{-1}), respectively. F is the flow rate of the exit gas on the sweep side (ml s^{-1}), and S is the membrane geometric surface area of the sweep side (cm^2).

3. Results

3.1. Basic properties

Fig. 2 shows the SEM morphologies of the freshly prepared powders (OP), and the powders after the further ball milling for 2 h (MP). Large amount of agglomerates are presented in the freshly prepared powders (Fig. 2a), which may be attributed to the bridging effect of strong polar groups contained in the powder precursor.[30] These large agglomerates are generally unfavorable for powder sintering.[31] MP is more loosely dispersed than OP (Fig. 2b), because large agglomerates were mostly eliminated by conducting the ball milling process. In

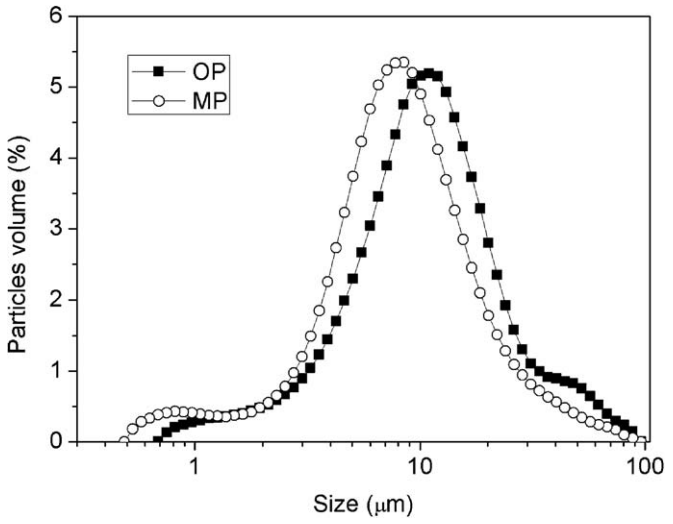

Fig. 3. The particle size distributions of the original powders (OP), and the ball-milled powders (MP).

addition, some flat-shape particles also appear in MP, which are recognized as a feature of wet milling.[20]

Original powders and ball-milled powders were further subjected for laser particle size distribution analysis with the results shown in Fig. 3. A smaller particle size for MP is observed than OP, which is in well agreement with the SEM observation. The two samples were further subjected to BET surface area measurement. The freshly prepared LSCF6428 powders (OP) have a specific surface area of 7.0 $m^2\ g^{-1}$, after 2 h of ball milling, the specific surface area of the powders (MP) increases to 17 $m^2\ g^{-1}$. Such increment can be explained by the breakage of hard agglomerates existed in OP after the ball milling.

Fig. 4 shows the room-temperature X-ray patterns for membranes sintered at 1100–1300 °C, utilizing original and ball-milled powders, respectively. It demonstrates that ball milling did not induce phase transition for the sintered membranes since all patterns can be indexed to the same cubic perovskite structure.

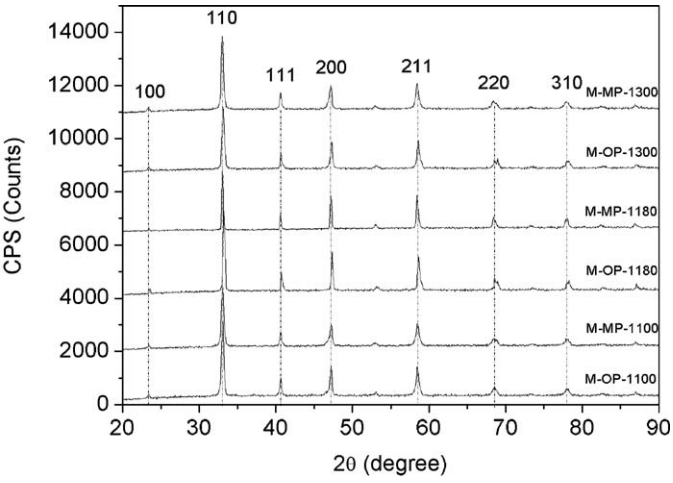

Fig. 4. The room-temperature X-ray patterns of the various membranes.

Fig. 5a shows the surface elemental composition of the milling balls. It can be seen that the milling balls are composed of Zr and O, and no impurity element was observed, indicating these balls are of high purity. Fig. 5b shows the bulk elemental composition of the sintered membranes utilizing the ball-milled powders. The spectra show a high purity level for the membranes. The peak for zirconium contamination from ball milling equipment (marked out at the vertical line) is not observed, demonstrating that very few impurities were introduced during the ball milling procedure.

The sintering properties of LSCF6428 membranes with and without the ball milling processes for the starting powders were investigated. Green membranes from OP and MP were first prepared by dry pressing and then sintered at different temperatures, and the relative density and linear shrinkage of the membranes were measured. After the sintering at 1100 °C, the membrane made from OP (M-OP-1100) only reaches a relative density at 86.1% (Table 1), and clearly presents lots of very tiny pores in the bulk (Fig. 6a). By applying ball milling to the original powders, the membrane sintering is promoted. As shown in Fig. 6d, M-MP-1100 reaches a relative density of 90.6%, and the bulk grains are tightly compacted, leaving less enclosed pores. For the membranes sintered at 1180 °C, both M-OP-1180 and M-MP-1180 are highly sintered with relative density reaching 91.7 and 93.2%, respectively. In addition, their grains are obviously larger than the membranes sintered at 1100 °C. With further comparison of Fig. 6b and e, it is found that the M-MP-1180 has larger grain size than the M-OP-1180, denoting the former is more sintered. For the membranes sintered at 1300 °C (Fig. 6c and f), both M-OP-1300 and M-MP-1300 are further sintered in terms of higher density (>95%) and larger grains formation as compared with membranes sintered at 1180 °C. Likewise, the membrane from ball-milled powders, i.e. M-MP-1300, has larger bulk grain size than M-OP-1300. Linear shrinkage of those sintered membranes was calculated through dividing the initial diameter of the green membrane by the decrement in diameter of the sintered membrane and the results recorded in percentage are listed in Table 1. It also clearly demonstrates the beneficial effect of the ball milling for the starting powders on the membrane sintering.

3.2. Oxygen permeation fluxes

Fig. 7a shows the temperature dependence of oxygen permeation fluxes through the various membranes made from OP sintered at different temperatures. It is noteworthy that the oxygen permeability for the LSCF6428 material under study is rather low compared with BSCF and BSZF materials, which is largely because the oxygen vacancy concentration for this material is low.[18,23,24] As can be seen, the M-OP-1100 shows an oxygen flux of 0.37 ml $cm^{-2}\ min^{-1}$ at 950 °C, while M-OP-1180 shows an improved flux of 0.51 ml $cm^{-2}\ min^{-1}$ at the same operation temperature. It is interesting that with the further increase of sintering temperature to 1300 °C, the oxygen permeation flux of the membrane (M-OP-1300) is only

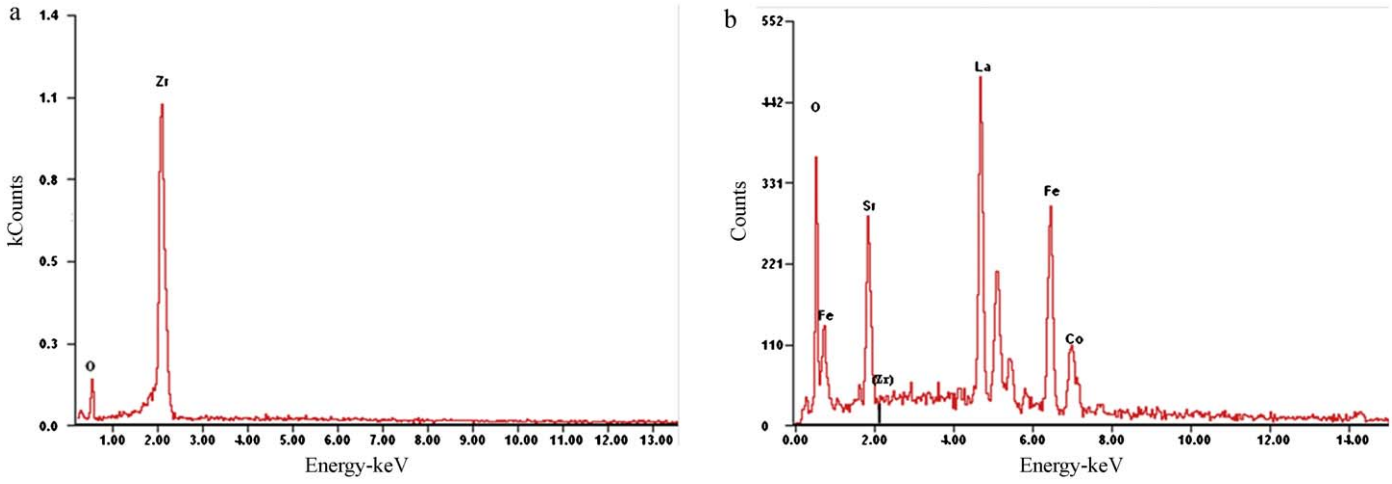

Fig. 5. The spectra of elemental composition of (a) the milling balls and (b) the sintered membranes utilizing ball-milled powders.

0.39 ml cm^{-2} min^{-1} at 950 °C, lower than that of M-OP-1180. Fig. 7b shows the temperature dependence of oxygen permeation flux through the membranes with the starting powders conducted the ball milling process (MP). It reaches a permeation flux of 0.43 ml cm^{-2} min^{-1} at operating temperature of 950 °C for the membrane sintered at 1100 °C, while they are 0.42 and 0.32 ml cm^{-2} min^{-1} for the membranes sintered at 1180 and 1300 °C, respectively. This trend is just the opposite to what we have found for the same LSCF6428 membrane with the powders synthesized from raw materials of lower purity level.[28]

4. Discussion

It is well known that high energy ball milling can reduce the average particle size and increase the sintering capability of ceramic.[32,33] Therefore, we applied ball milling to LSCF6428 powders to assist the membrane sintering. As it is observed above, the ball milling treatment has effectively broken down agglomerates into very fine particles which are essential to achieve high initial density for subsequent sintering.[34–37] Further, Pavlović et al. observed an improved sintering in terms of less pores and polyhedral grain formation when using

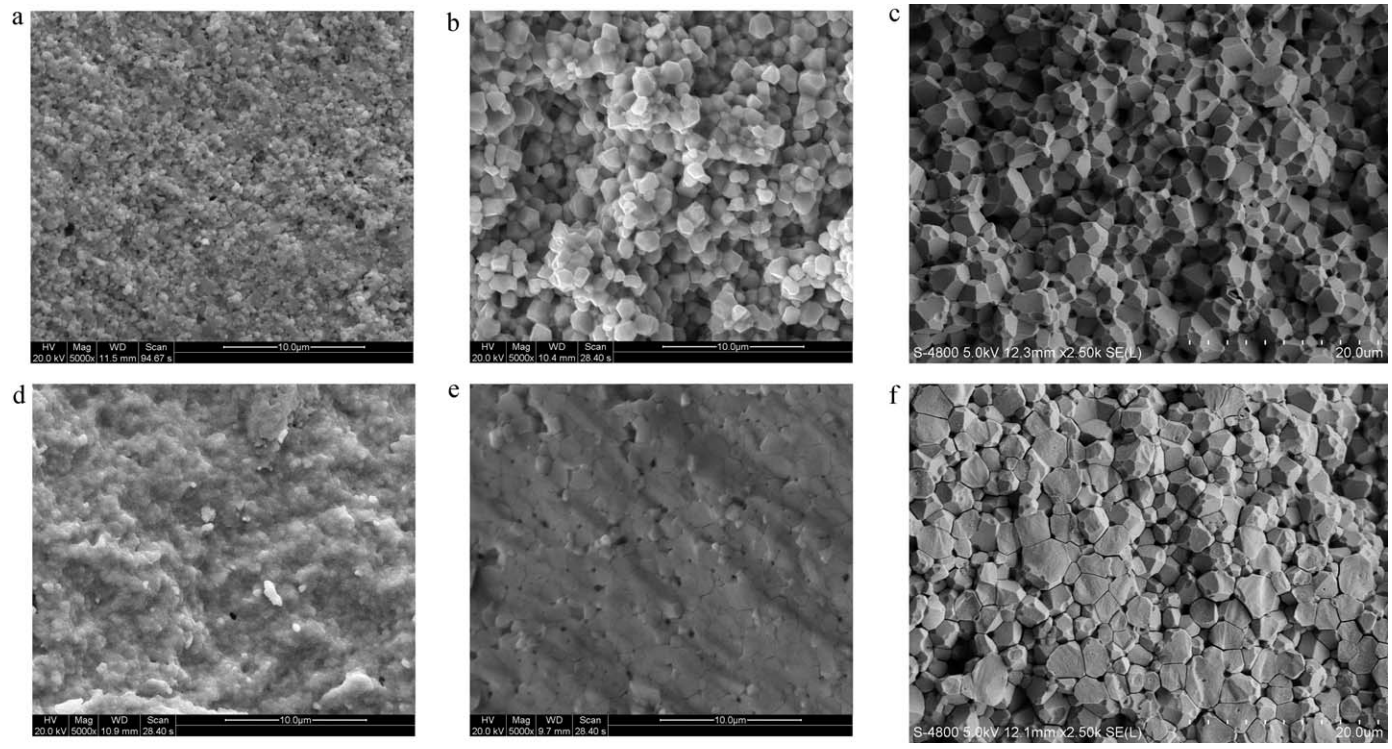

Fig. 6. The bulk morphologies of membranes made from the original and ball-milled powders: (a) M-OP-1100, (b) M-OP-1180, (c) M-OP-1300, (d) M-MP-1100, (e) M-MP-1180, and (f) M-MP-1300.

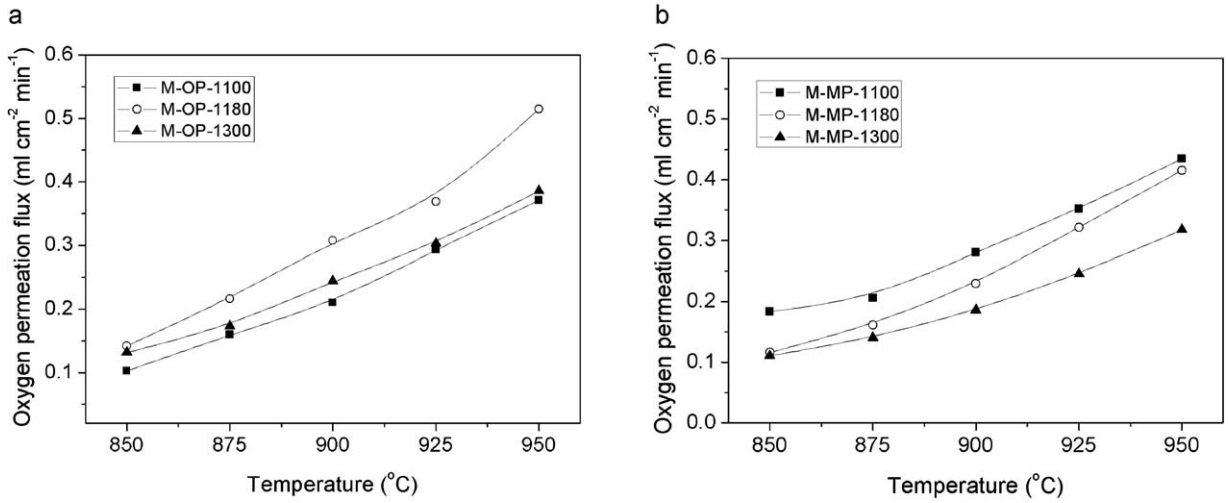

Fig. 7. The oxygen permeation plot versus temperature for membranes made from: (a) the original powders and (b) the ball-milled powders.

ball-milled powders that are mechanically activated.[38] Our results agree pretty well with their conclusions. To this end, we attribute the oxygen permeability increase for M-MP-1100 to the less porous microstructure which reduces the effect of pore block on mass transport. Therefore, ball milling is a facile way to increase the sintering of ceramic membranes.

Previously we have demonstrated an increase in oxygen permeation flux for the LSCF6428 membrane with the increase of sintering temperature, which resulted in an increase in the grain size, while the sintering density was not obviously affected, and we further proposed that the grain boundaries blocked the diffusion of oxygen ion.[28] In this study, for the membranes prepared from starting powders without conducting the ball milling process (OP), the higher flux of M-OP-1180 ($\sim$0.51 ml cm^{-2} min^{-1}) than M-OP-1100 (0.37 ml cm^{-2} min^{-1}) can be explained at least in part from the increased sintering density, i.e. from 86.1% to 91.7%. However, the lower permeation flux (at 950 °C) of M-OP-1300 (0.39 ml cm^{-2} min^{-1}) than M-OP-1180 (0.51 ml cm^{-2} min^{-1}) strongly suggests the grain boundaries are beneficial for the oxygen ion diffusion since these two membranes have similar sintering density while the former (M-OP-1180) has smaller grain size than the later (M-OP-1300), as shown in Fig. 6b and c.

By applying ball milling process, the sinterability of the powders is greatly improved; as a result, the sintering density of M-MP-1100 also reaches a high level of 90.6%. Thus the effect of the sintering density on the oxygen permeation of the membranes should be less significant. As shown in Fig. 7b, for the membranes sintered between 1100 and 1300 °C with MP as the starting powders, a decrease in permeation flux with the increase of sintering temperature was demonstrated. According to Fig. 6d–f, the increase in sintering temperature results in the increase of grain size. It thus further implies that the grain boundaries facilitate the oxygen diffusion. These results are consistent with what Benson SJ have reported.[39] The opposite effect of grain boundaries on the oxygen permeation flux from our previous report can be explained by the blocking effect of impurity phase around the grain boundaries.

In order to verify this grain-boundary and oxygen-permeability relationship, we also examined the membranes sintered at the same temperature. Fig. 8 shows the bulk grain size distributions of these membranes. Bulk grains in M-OP-1180 membrane mainly peak at $\sim$0.75 μm with a notable proportion bellow 0.5 μm and a slight amount over 1.0 μm (Fig. 8a), resulting in a broad grain size distribution, which may be related to the existence of agglomerates in fresh powders.[26] It is noteworthy that the tiny grains also take a shape close to sphere (Fig. 6b), indicating that only an initial stage of grain growth took place. For M-MP-1180 membrane (Fig. 6e), the grain size mainly distributes around 1.0 μm (Fig. 8b), and the amount of small grains is obviously reduced. It is also characterized by the polyhedral grain shape, implying a full development of grain growth, as suggested by Gottstein et al.[40] So these evidences of grain growth demonstrate that M-MP-1180 has less grain boundary areas than M-OP-1180. It thus further supports the grain boundaries facilitate the oxygen diffusion. A comparison of oxygen permeability between M-OP-1300 and M-MP-1300 was also made. As expected, oxygen permeability of M-MP-1300 (0.32 ml cm^{-2} min^{-1} at 950 °C) was lower than M-OP-1300 (0.39 ml cm^{-2} min^{-1} at 950 °C), accompanied by an increase in average grain size as shown in Fig. 8c and d. From above analysis, it turns out that 1100 °C is the optimal sintering temperature for the membranes utilizing ball-milled powders, since it achieves relatively high density without causing obvious grain growth.

In our previous work, an increase in oxygen permeation flux was observed for LSCF6428 membranes with the increase of grain size, while an opposite conclusion was clearly demonstrated in current study. Previously we used conventional analytical reagents with purity of >99.5%, while in this study, the raw materials are in high purity with purity >99.99%. The main difference of the LSCF6428 membranes between those two studies is the purity of the raw materials. Thus it is clear that

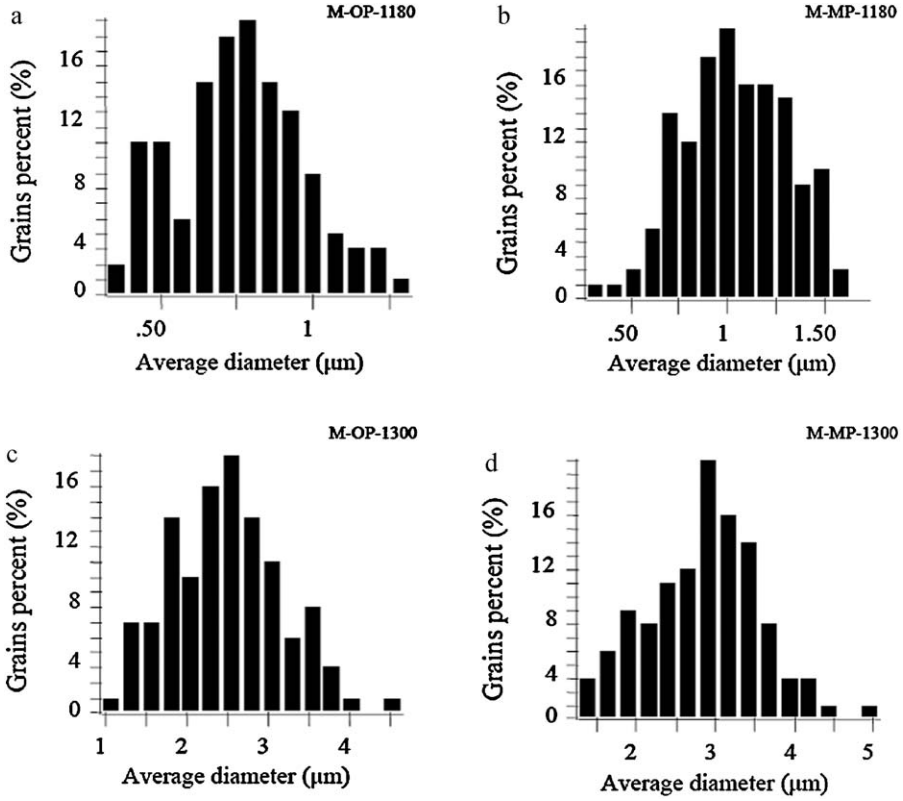

Fig. 8. The bulk grain size distributions for sintered membranes: (a) M-OP-1180, (b) M-MP-1180, (c) M-OP-1300, and (d) M-MP-1300.

the impurity phases have significant effect on the oxygen transportation through the ceramic membranes. Thus, the powder synthesis is one important procedure which should be carefully taken into consideration in the study on materials for oxygen separation.

5. Conclusions

The synthesized $La_{0.6}Sr_{0.4}Co_{0.2}Fe_{0.8}O_{3-\delta}$ (LSCF6428) powders from high-purity raw materials need a sintering temperature above 1180 °C to achieve sufficient density (>90%). Applying High energy ball milling (HEBM) to the original LSCF6428 powders can effectively improve the powder sinterability, increasing the membrane density from 86.1 to 90.6% at a sintering temperature of 1100 °C. For the as prepared membranes, an increase in permeation flux with the decrease of grain size was demonstrated, just opposite to our previous observation. Dependence of oxygen permeation flux on the grain size evidences the fact that grain boundaries facilitate oxygen diffusion. The opposite conclusion in our previous study is due to the impurity phases accumulated at grain boundaries, which likely caused blocks for the grain boundary diffusion of electron and ion, as previously proposed. Ball milling treatment of the original powders leads to the decrease in oxygen permeability with the increase of membrane sintering temperature, due to obvious bulk grain growth. The sintering temperature of 1100 °C turns out to be optimal for the membrane with ball-milled powders as the starting material. It suggests, besides the materials composition, both the powder synthesis and membrane sintering strategies are also crucial in order to achieve high oxygen permeation flux of mixed conducting membranes.

Acknowledgements

This work was supported by the "China National Funds to Distinguished Young Scientists" under contract no. 51025209, the "Outstanding Young Scholar Grant at Jiangsu Province" under contract no. 2008023, the Fok Ying Tung Education Grant under contract no. 111073, Program for New Century Excellent Talents in Chinese Ministry of Education, the National Basic Research Program of China under contract no. 2007CB209704.

References

1. *Basic energy science [Internet]*. Washington DC: U.S. DOE, Office of science. Available from: http://science.energy.gov/bes/ [cited 02.03.11].
2. Tan Y, Douglas MA, Thambimuthu KV. CO_2 capture using oxygen enhanced combustion strategies for natural gas power plants. *Fuel* 2002;**81**:1007–16.
3. Bisio G, Bosio A, Rubatto G. Thermodynamics applied to oxygen enrichment of combustion air. *Energy Convers Manage* 2002;**43**:2589–600.
4. Gupta PK. An analysis of oxygen enrichment of combustion air in fossil fuel fired glass melting tanks. *J Non-Cryst Solids* 1980;**38**(9):761–6.
5. Ainsworth S. Oxygenates seen as hot market by industry. *Chem Eng News* 1992;**70**:26–30.
6. Teraoka Y, Zhang H, Furukawa S, Yamazoe N. Oxygen permeation through perovskite-type oxides. *Chem Lett* 1985;**11**:1743–6.
7. Kharton VV, Naumovich EN, Nikolaev AV. Materials of high-temperature electrochemical oxygen membranes. *J Membr Sci* 1996;**111**:149–57.
8. Ishihara T, Matsuda H, Takita Y. Doped $LaGaO_3$ perovskite type oxide as a new oxide ionic conductor. *J Am Chem Soc* 1994;**116**:3801–3.

9. Kilner J, Benson S, Lane J, Waller D. Ceramic ion conducting membranes for oxygen separation. *Chem Ind* 1997;**17**:907–11.
10. Ten Elshof JE, Bouwmeester HJM, Verweij H. Oxidative coupling of methane in a mixed-conducting perovskite membrane reactor. *Appl Catal A* 1995;**130**:195–212.
11. Kharton VV, Viskup AP, Marozau IP, Naumovich EN. Oxygen permeability of perovskite-type $Sr_{0.7}Ce_{0.3}MnO_{3-\delta}$. *Mater Lett* 2003;**57**:3017–21.
12. Kharton VV, Marques FMB. Mixed ionic–electronic conductors: effects of ceramic microstructure on transport properties. *Curr Opin Solid State Mater Sci* 2002;**6**:261–9.
13. Maier J. Transport in electroceramics: micro- and nano-structural aspects. *J Eur Ceram Soc* 2004;**24**:1251–7.
14. Diethelm S, Herle JV, Sfeir J, Buffat P. Correlation between oxygen transport properties and microstructure in $La_{0.5}Sr_{0.5}FeO_{3-\delta}$. *J Eur Ceram Soc* 2005;**25**:2191–6.
15. Kusaba H, Shibata Y, Sasaki K, Teraoka Y. Surface effect on oxygen permeation through dense membrane of mixed-conductive LSCF perovskite-type oxide. *Solid State Ionics* 2006;**177**:2249–53.
16. Zhang K, Yang YL, Ponnusamy D, Jacobson AJ, Salama K. Effect of microstructure on oxygen permeation in $SrCo_{0.8}Fe_{0.2}O_{3-\delta}$. *J Mater Sci* 1999;**34**:1367–72.
17. Shaula AL, Fuentes RO, Figueiredo FM, Kharton VV, Marques FMB, Frade JR. Grain size effects on oxygen permeation in submicrometric $CaTi_{0.8}Fe_{0.2}O_{3-\delta}$ ceramics obtained by mechanical activation. *J Eur Ceram Soc* 2005;**25**:2613–6.
18. Arnold M, Martynczuk J, Efimov K, Wang HH, Feldhoff A. Grain boundaries as barrier for oxygen transport in perovskite-type membranes. *J Membr Sci* 2008;**316**:137–44.
19. Martynczuk J, Arnold M, Feldhoff A. Influence of grain size on the oxygen permeation performance of perovskite-type $(Ba_{0.5}Sr_{0.5})(Fe_{0.8}Zn_{0.2})O_{3-\delta}$ membranes. *J Membr Sci* 2006;**322**:375–82.
20. Baumann S, Schulze-Küppers F, Roitsch S, Betz M, Zwick M, Pfaff EM, et al. Influence of sintering conditions on microstructure and oxygen permeation of $Ba_{0.5}Sr_{0.5}Co_{0.8}Fe_{0.2}O_{3-\delta}$ (BSCF) oxygen transport membranes. *J Membr Sci* 2010;**359**:102–9.
21. Wang H, Tablet C, Feldhoff A, Caro J. Investigation of phase structure, sintering, and permeability of perovskite-type $Ba_{0.5}Sr_{0.5}Co_{0.8}Fe_{0.2}O_{3-\delta}$ membranes. *J Membr Sci* 2005;**262**:20–6.
22. Ge L, Zhou W, Ran R, Shao ZP, Liu SM. Facile autocombustion synthesis of $La_{0.6}Sr_{0.4}Co_{0.2}Fe_{0.8}O_{3-\delta}$ (LSCF) perovskite via a modified complexing sol–gel process with NH_4NO_3 as combustion aid. *J Alloy Compd* 2008;**450**:338–47.
23. Ge L, Zhu ZH, Shao ZP, Wang SB, Liu SM. Effects of preparation methods on the oxygen nonstoichiometry, B-site cation valences and catalytic efficiency of perovskite $La_{0.6}Sr_{0.4}Co_{0.2}Fe_{0.8}O_{3-\delta}$. *Ceram Int* 2009;**35**:3201–6.
24. Lane JA, Benson SJ, Waller D, Kilner JA. Oxygen transport in $La_{0.6}Sr_{0.4}Co_{0.2}Fe_{0.8}O_{3-\delta}$. *Solid State Ionics* 1999;**121**:201–8.
25. Cox-Galhotra RA, McIntosh S. Unreliability of simultaneously determining k_{chem} and D_{chem} via conductivity relaxation for surface-modified $La_{0.6}Sr_{0.4}Co_{0.2}Fe_{0.8}O_{3-\delta}$. *Solid State Ionics* 2010;**181**:1429–36.
26. Tan XY, Wang ZG, Liu H, Liu SM. Enhancement of oxygen permeation through $La_{0.6}Sr_{0.4}Co_{0.2}Fe_{0.8}O_{3-\delta}$ hollow fibre membranes by surface modifications. *J Membr Sci* 2008;**324**:128–35.
27. Wang S, van der Heide PAW, Chavez C, Jacobson AJ, Adler SB. An electrical conductivity relaxation study of $La_{0.6}Sr_{0.4}Co_{0.2}Fe_{0.8}O_{3-\delta}$. *Solid State Ionics* 2003;**156**:201–8.
28. Zeng PY, Ran R, Cheng ZH, Gu HX, Shao ZP. Significant effects of sintering temperature on the performance of $La_{0.6}Sr_{0.4}Co_{0.2}Fe_{0.8}O_{3-\delta}$ oxygen selective membranes. *J Membr Sci* 2007;**302**:171–9.
29. Zhang K, Ran R, Ge L, Shao ZP, Jin WQ, Xu NP. Systematic investigation on new $SrCo_{1-y}Nb_yO_{3-\delta}$ ceramic membranes with high oxygen semipermeability. *J Membr Sci* 2008;**323**:436–43.
30. Kim DW, Kim DS, Kim YG, Kim YC, Oh SG. Preparation of hard agglomerates free and weakly agglomerated antimony doped tin oxide (ATO) nanoparticles by coprecipitation reaction in methanol reaction medium. *Mater Chem Phys* 2006;**97**:452–7.
31. Groza JR, Dowding RJ. Nanoparticluate materials densification. *Nanostruct Mater* 1996;**7**:749–68.
32. Li HB, Xia CR, Zhu MH, Zhou ZX, Wei XL, Meng GY. Increasing the sinterability of tape cast oxalate-derived doped ceria powder by ball milling. *Ceram Int* 2007;**33**:201–5.
33. Kong LB, Ma J, Zhu W, Tan OK. Reaction sintering of partially reacted system for PZT ceramics via a high-energy ball milling. *Scr Mater* 2001;**44**:345–50.
34. Hennart SLA, Wildeboer WJ, van Hee P, Meesters GMH. Identification of the grinding mechanisms and their origin in a stirred ball mill using population balances. *Chem Eng Sci* 2009;**64**:4123–30.
35. Chol GR. Influence of milled powder particle size distribution on the microstructure and electrical properties of sintered Mn–Zn ferrites. *J Am Ceram Soc* 1971;**54**:34–9.
36. Kanters J, Eisele U, Rödel J. Effect of initial grain size on sintering trajectories. *Acta Mater* 2000;**48**:1239–46.
37. Zheng JM, Reed JS. Effects of particle packing characteristics on solid-state sintering. *J Am Ceram Soc* 1989;**72**:810–7.
38. Pavlović VP, Nikolić MV, Nikolić Z, Branković G, Živković L, Pavlović VB, et al. Microstructural evolution and electric properties of mechanically activated $BaTiO_3$ ceramics. *J Eur Ceram Soc* 2007;**27**:575–9.
39. Benson SJ, Chater RJ, Kilner JA. Oxygen diffusion and surface exchange in the mixed conducting perovskite $La_{0.6}Sr_{0.4}Co_{0.2}Fe_{0.8}O_{3-\delta}$. In: *Proceedings of the 3rd International Symposium on Ionic and Mixed Conducting Ceramics, PV 97-24*. Pennington: The Electrochemical Society; 1998. p. 596–609.
40. Gottstein G, King AH, Shvindlerman LS. The effect on triple junction drag on grain growth. *Acta Mater* 2000;**48**:397–403.